

Stochastic thermodynamics of chemical reactions coupled to finite reservoirs: A case study for the Brusselator

Jonas H. Fritz,¹ Basile Nguyen,¹ and Udo Seifert^{1, a)}

II. Institut für Theoretische Physik, Universität Stuttgart, 70550 Stuttgart, Germany

(Dated: 3 January 2022)

Biomolecular processes are typically modeled using chemical reaction networks coupled to infinitely large chemical reservoirs. A difference in chemical potential between these reservoirs can drive the system into a non-equilibrium steady state (NESS). In reality, these processes take place in finite systems containing a finite number of molecules. In such systems, a NESS can be reached with the help of an externally driven pump for which we introduce a simple model. Crucial parameters are the pumping rate and the finite size of the chemical reservoir. We apply this model to a simple biochemical oscillator, the Brusselator, and quantify the performance using the number of coherent oscillations. As a surprising result, we find that higher precision can be achieved with finite-size reservoirs even though the corresponding current fluctuations are larger than in the ideal infinite case.

I. INTRODUCTION

Biological systems require a constant supply of energy to perform their tasks. There are numerous examples from molecular motors^{1–4} such as kinesin or myosin to biological switches and oscillators such as the circadian clock^{5,6}, the MinDE system^{7–11} or the interlinked GTPase cascade^{12–15}. All of these systems reach a non-equilibrium steady state (NESS) by extracting energy from nucleotide phosphates such as adenosine or guanosine triphosphate (ATP or GTP)^{16,17}. Chemical energy is released through a hydrolysis reaction which breaks one of the phosphate bonds (dephosphorylation) and converts a nucleotide triphosphate (ATP) into a nucleotide diphosphate (ADP, GDP) and an inorganic phosphate (P_i). The thermodynamic models which describe these systems generally rely on infinitely large reservoirs that supply these species at a fixed concentration, which are called chemostats. In reality, these processes take place in finite systems with a finite number of molecules. As a consequence, real biological oscillators do not have infinitely big chemostats at their disposal.

Instead, living systems rely on cellular respiration, a metabolic process that recycles ADP into ATP^{18,19} in order to remain in a NESS. It starts with glycolysis which converts glucose into pyruvates, then a series of oxidative phosphorylation results in the pumping of protons across the mitochondrial membrane creating an electrochemical gradient. The final recycling step is performed by a rotary molecular motor, namely the ATP synthase or F_0F_1 -ATPase in bacteria^{20,21}. The main purpose of this molecular motor is to maintain a NESS for different processes in the cell. The F_0 -part is embedded in the membrane and couples to the proton gradient to rotate a central shaft. The F_1 -motor uses ATP hydrolysis to rotate in the opposite direction. By coupling the two parts with a strong enough proton gradient, the F_1 -motor ro-

tates in reverse and thereby synthesizes ATP from ADP and P_i . Experimental techniques have enabled the observations of individual trajectories at the single molecule level^{22–24}. From such trajectories, efficiencies for the motor could be computed^{25–27}.

In this paper, we replace the chemostats with finite reservoirs and add a simple reaction scheme that fulfills a similar role to the F_0F_1 -ATPase. Reactions in which a molecule leaves or enters the finite reservoir will change its concentration depending on the bath size. We quantify this effect with a parameter Λ which describes how large the bath is compared to the rest of the system. The change in concentration is inversely proportional to the bath size, so in the limit $\Lambda \rightarrow \infty$ the change vanishes and we recover the ideal reservoir. We choose a simple unimolecular driven reaction with reaction speed γ to mimic the role of the F_0F_1 -ATPase in cells. This reaction upholds the chemical free energy difference between the reservoirs. In a different context, a finite-size temperature bath has been considered in^{28,29} where it was modeled as a set of independent linear oscillators.

We investigate how these modifications impact biochemical oscillators by considering the Brusselator model as a case study for how finite chemical reservoirs affect the performance of biological systems. Naively, one may expect that finite reservoirs would introduce additional noise into the system and lead to a decrease of its quality. We show that a simple biochemical oscillator with finite reservoirs can achieve higher precision than its counterpart with ideal reservoirs despite the increase in fluctuations. The relation between the precision of biochemical oscillations and the energy required to sustain them has received much attention recently for ideal reservoirs^{30–39}.

This paper is organized as follows. In Section II, we introduce a Brusselator model and its modified version with a pumping mechanism. In Section III, we show that higher precision can be achieved with finite reservoirs despite showing larger fluctuations. We find that there is an optimal reservoir size and pumping speed which outperforms the ideal reservoir case. We conclude in Section IV.

^{a)} For correspondence: useifert@theo2.physik.uni-stuttgart.de

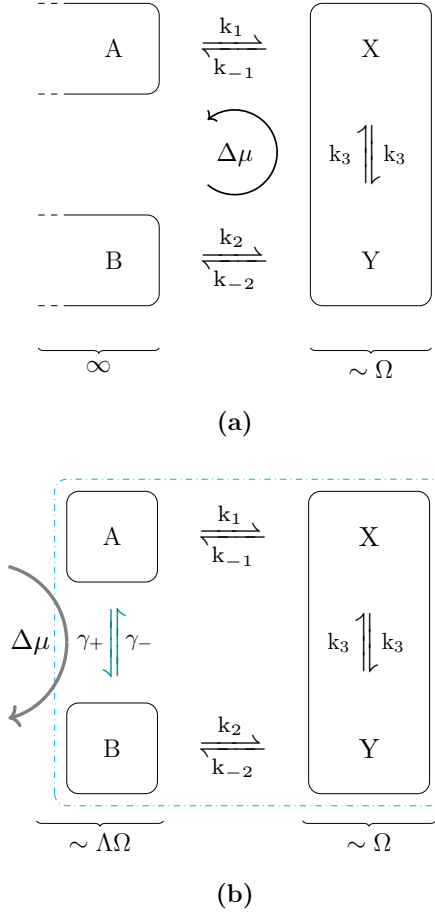


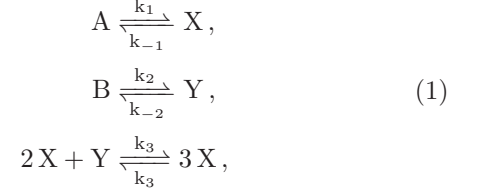
FIG. 1. Comparison of the Brusselator (a) and our modified version with finite reservoirs (b). In (b) species A and B are part of the system. Their finite size scales with both with the system size Ω and Λ which quantifies how large the size of the reservoirs is compared with the system size Ω . Ideal reservoirs are recovered in the limit $\Lambda \rightarrow \infty$. To uphold the NESS an additional driven reaction scheme γ_{\pm} highlighted in green is introduced. The dashdotted blue box separates the inside of the finite system from the outside from where the pump is fueled.

II. MODELS

A. The Brusselator model

The Brusselator is arguably the simplest set of chemical reactions that can exhibit oscillations as sketched in Fig. 1 (a). It consists of two chemical species X and Y in a volume Ω . X and Y molecules can be produced from chemostats containing A and B molecules, respectively.

The set of chemical reactions is



where the k_1, k_{-1}, k_2, k_{-2} and k_3 are transition rates. This reaction scheme, first considered in⁴⁰ is a modified version of the original Brusselator^{41,42}. Through a chemical free energy difference $\Delta\mu$ between the chemostats the system is driven out of equilibrium into a NESS. Thermodynamic consistency requires the rates k_i and $\Delta\mu \equiv \mu_B - \mu_A$ to be related via the local detailed balance condition, which in this case reads

$$e^{\Delta\mu} = \frac{[B]k_2k_{-1}}{[A]k_{-2}k_1}, \quad (2)$$

where we set $\beta = 1$ throughout this paper⁴³. The thermodynamic force $\Delta\mu$ must be above a certain critical threshold $\Delta\mu_c$ for biochemical oscillations to set in^{31,33}.

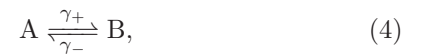
B. The Brusselator with finite reservoirs

In the model with infinite reservoirs, the concentrations $[A]$ and $[B]$ remain constant, i.e., are chemostatted. For finite reservoirs this is no longer the case. The number of A and B molecules will now be part of the system and changes according to the set of chemical reactions. We introduce a parameter Λ , which characterizes the size of the reservoirs compared with the system size Ω . The initial number of molecules in the bath is given by (1)

$$\begin{aligned} n_A &= [A] \Lambda \Omega, \\ n_B &= [B] \Lambda \Omega, \end{aligned} \quad (3)$$

where $[A]$ and $[B]$ are the chemostatted concentrations from the original model. The total number of molecules $N_{\text{tot}} = n_X + n_Y + n_A + n_B$ becomes a conserved quantity.

In such a system, the NESS can be maintained by an externally driven pump. This driving has to be supplied by external ideal reservoirs, which are outside the dash-dotted blue box in Fig. 1 (b). In the case of the ATP synthase, the ideal reservoirs correspond to the the proton gradient. The NESS is reached by the pump sustaining a chemical gradient between A and B. The simplest possible reaction scheme achieving this feature is



where γ_{\pm} are transition rates, see Fig. 1 (b). With this additional reaction, the local detailed balance condition reads

$$e^{\Delta\mu} = \frac{\gamma_+ k_2 k_{-1}}{\gamma_- k_{-2} k_1}. \quad (5)$$

We assume that the rates k_i are fixed, thus Eq. (5) relates the ratio of γ_+ and γ_- to a given $\Delta\mu$. As a free parameter, we choose $\gamma \equiv \gamma_+$, which is the characteristic timescale of the pump. Our modified model is then described by three parameters: the size ratio Λ , the speed of the pump γ and the chemical free energy difference

$\Delta\mu$.

C. Chemical master equation and deterministic equations

The evolution of the probability to find the system in a state $\mathbf{n} \equiv (n_X, n_Y, n_A, n_B)$ at time t is described by the chemical master equation (CME)⁴⁴

$$\begin{aligned} \partial_t P(\mathbf{n}, t) = & \left\{ k_1 [(n_A + 1)\epsilon_X^- \epsilon_A^+ - n_A] + k_2 [(n_B + 1)\epsilon_Y^- \epsilon_B^+ - n_B] \right. \\ & + k_{-1} [(n_X + 1)\epsilon_X^+ \epsilon_A^- - n_X] + k_{-2} [(n_Y + 1)\epsilon_Y^+ \epsilon_B^- - n_Y] \\ & + \frac{k_3}{\Omega^2} [(n_X - 1)(n_X - 2)(n_Y + 1)\epsilon_X^- \epsilon_Y^+ + (n_X + 1)n_X(n_X - 1)\epsilon_X^+ \epsilon_Y^- \\ & - n_X(n_X - 1)n_Y - n_X(n_X - 1)(n_X - 2)] \\ & \left. + \gamma^+ [(n_A + 1)\epsilon_A^+ \epsilon_B^- - n_A] + \gamma^- [(n_B + 1)\epsilon_B^+ \epsilon_A^- - n_B] \right\} P(\mathbf{n}, t), \end{aligned} \quad (6)$$

where we define the step operators as

$$\begin{aligned} \epsilon_X^\pm P(\mathbf{n}, t) &\equiv P(n_X \pm 1, n_Y, n_A, n_B, t), \\ \epsilon_Y^\pm P(\mathbf{n}, t) &\equiv P(n_X, n_Y \pm 1, n_A, n_B, t), \\ \epsilon_A^\pm P(\mathbf{n}, t) &\equiv P(n_X, n_Y, n_A \pm 1, n_B, t), \\ \epsilon_B^\pm P(\mathbf{n}, t) &\equiv P(n_X, n_Y, n_A, n_B \pm 1, t). \end{aligned} \quad (7)$$

In the deterministic limit ($\Omega \rightarrow \infty$), we obtain from Eq. (6) the rate equations for the concentrations,

$$I \equiv \sum_{\mathbf{n}} n_I P(\mathbf{n}, t) / \Omega \quad I \in \{X, Y, A, B\}. \quad (8)$$

as

$$\begin{aligned} \dot{X} &= k_1 A - k_{-1} X + k_3 (X^2 Y - X^3), \\ \dot{Y} &= k_2 B - k_{-2} Y + k_3 (X^3 - X^2 Y), \\ \dot{A} &= -k_1 A + k_{-1} X - \gamma_+ A + \gamma_- B, \\ \dot{B} &= -k_2 B + k_{-2} Y + \gamma_+ A - \gamma_- B. \end{aligned} \quad (9)$$

D. Stochastic simulations

We have performed continuous time Monte Carlo simulations of Eq. (6) using Gillespie's algorithm⁴⁵. For all simulations we set the parameters to $\Omega = 1000$, $k_1 = 0.1/\Lambda$, $k_{-1} = 0.1$, $k_2 = 0.1/\Lambda$, $k_{-2} = 0.003$, $k_3 = 0.001$ and $N_{\text{tot}} = 7.5 \cdot \Omega \cdot \Lambda$. Here, Λ is dimensionless parameter that reflects how large $n_A + n_B$ is compared to $n_X + n_Y$. We include Λ in the total number of molecules. We also choose to scale the rates k_1 and k_2 with a factor $1/\Lambda$ in order to make the reaction propensities $k_1 n_A$ and $k_2 n_B$ independent of Λ . This ensures that we recover the ideal reservoirs dynamics in the limit $\Lambda \rightarrow \infty$. We choose $\Delta\mu$, γ and Λ as control parameters.

E. Precision of oscillations and diffusion coefficient

In Fig. 2(a), we plot an example of an oscillating trajectory for species X and B. Such oscillations occur in systems with a finite number of molecules that display large fluctuations. To quantify the precision of oscillations, we compute the correlation function for species X which is defined as

$$\begin{aligned} C_X(t) &\equiv \frac{\langle (n_X(t) - \langle n_X \rangle) (n_X(0) - \langle n_X \rangle) \rangle}{\langle n_X^2 \rangle - \langle n_X \rangle^2} \\ &\approx \exp(-t/\tau_c) \cos(2\pi t/T), \end{aligned} \quad (10)$$

where the bracket denote an average over stochastic trajectories. We obtain the correlation time τ_c and the period length T by fitting the correlation function numerically with the function given in the second line of Eq. (10). In Fig. 2(b), we show a typical correlation function in the oscillating regime. The number of coherent oscillations is defined as the correlation time divided by the period length, i.e.,

$$\mathcal{N} \equiv \frac{\tau_c}{T}. \quad (11)$$

It measures how long different realizations of the oscillator stay coherent with each other. Thus \mathcal{N} is a natural choice to quantify the precision of biochemical oscillations^{30,32}.

As a measure for fluctuations, we consider the current conjugated to the thermodynamic force $\Delta\mu$, which is related to the entropy production. In the model with infinite reservoirs, this current is given by the rate of consumption of B. In our modified model, the thermodynamic flux is related to the pumping scheme (4). We can analyse its fluctuations by considering the stochastic time-integrated current Z . In a stochastic trajectory,

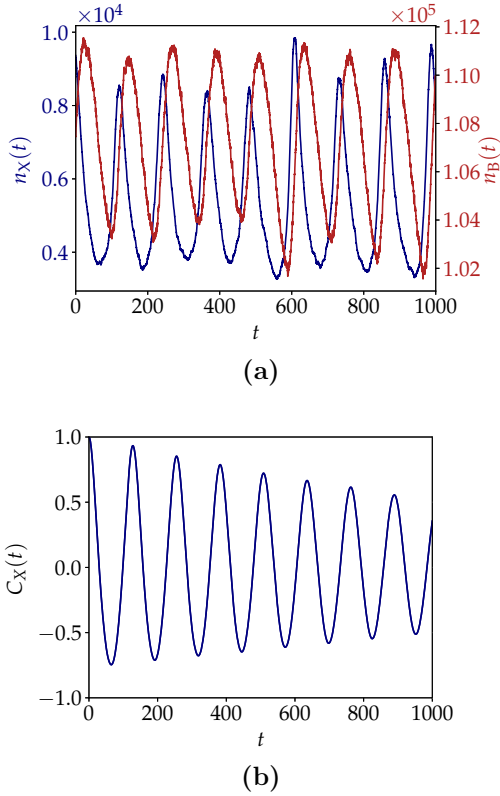
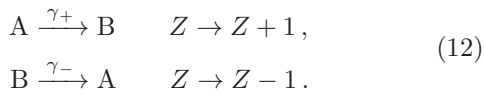


FIG. 2. Stochastic trajectories of the Brusselator with finite reservoirs. (a) Trajectory of the number of X molecules n_X (blue) and B molecules n_B (red) where we set $\Lambda = 20$, $\Delta\mu = 5.5$, $\gamma = 1$. The remaining parameters are given in the main text. (b) Correlation function, fitted with Eq. (10), leading to $\mathcal{N} \simeq 10$ coherent oscillations.

this random variable increases by one if a A is converted to an B molecule, which happens if the transition with rate γ_+ takes place. Likewise Z decreases by one if an B is converted to a A molecule, which happens if the transition with rate γ_- takes place, i.e.,



The average thermodynamic flux is then defined as

$$J \equiv \lim_{\mathcal{T} \rightarrow \infty} \frac{\langle Z \rangle}{\mathcal{T}\Omega}. \quad (13)$$

where \mathcal{T} is the sampling time interval. Note that we choose our system parameters such that J does not depend on the reservoir size Λ , this is due to the scaling factor $1/\Lambda$ in the rates k_1 and k_2 . In the steady-state, the rate of entropy production is simply given by $\sigma \equiv J\Delta\mu$. The fluctuations can be quantified by the diffusion coefficient, which is defined as

$$D \equiv \lim_{\mathcal{T} \rightarrow \infty} \frac{\langle Z^2 \rangle - \langle Z \rangle^2}{2\Omega\mathcal{T}}, \quad (14)$$

At the onset of oscillations, this quantity diverges as a power-law with the system size³³. Interestingly, D has a universal lower bound that depends only on the thermodynamic force $\Delta\mu$, which follows from the thermodynamic uncertainty relation^{46–48}. We choose D as a quantifier for the fluctuations of the system.

III. RESULTS

A. Deterministic equations

We first consider the deterministic Eq. (9) and study its non-equilibrium steady state solutions for which the left-hand side vanishes. These equations are solved numerically. We obtain the phase diagrams shown in Fig. 3, we plot the amplitude of oscillations defined as follows,

$$\text{Amplitude} = \frac{\max(X(t)) - \min(X(t))}{\langle X \rangle} \equiv \frac{X_{\max} - X_{\min}}{\langle X \rangle}. \quad (15)$$

In all three cross sections there is an interplay between the parameters. For example, in Fig. 3(a), if the finite reservoir size ratio Λ is too large for a fixed $\Delta\mu$ the oscillations may vanish. A too large thermodynamic force $\Delta\mu$ for a fixed Λ can also make the oscillations vanish. We observe the same effect in Fig. 3(b) for γ , namely, a range of possible timescales for the pump that leads to oscillations. In Fig. 3(c) the interplay is most crucial: increasing both $\Delta\mu$ and γ too far simultaneously makes oscillations vanish as well. Note that this effect, which is due to an additional fixed-point, is different from the case where $\Delta\mu$ or γ are too small. In the latter case, the system goes through a Hopf bifurcation, where the amplitude vanishes at the critical point. This difference can be seen qualitatively by the fact that the amplitude is different along the boundaries where oscillations vanish as will be explained in detail later.

B. CME

We now consider oscillations in a system with a finite number of molecules that can display large fluctuations. We choose the diffusion coefficient D , Eq. (14), to quantify the fluctuations of the system and the number of coherent oscillations \mathcal{N} , Eq. (11), to quantify the precision of oscillations. In Fig. 4, we plot the diffusion coefficient D and the number of coherent oscillations \mathcal{N} along the arrows shown in Fig. 3. At the phase transition, the diffusion coefficient has a local maximum³³. Surprisingly, we observe that both \mathcal{N} and D increase simultaneously, in other words, higher precision can be achieved with stronger fluctuations. This is in contrast to the Brusselator model³³ and unicyclic models^{49,50}. The same feature, however, is shared by other models, such as the activator-inhibitor model³³. In this sense, \mathcal{N} and D are not always strongly correlated in biochemical oscillators.

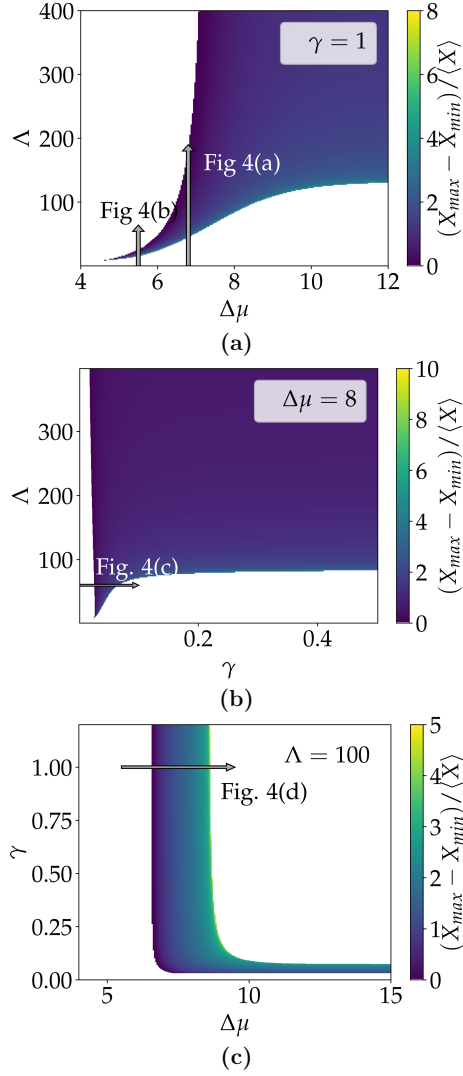


FIG. 3. Three different cross sections of the $\Delta\mu$ - γ - Λ phase-space. The amplitude of oscillations $(X_{\max} - X_{\min}) / \langle X \rangle$ is color coded. The white space indicates that no oscillations occur.

What causes oscillations to vanish? First, $\Delta\mu$ must be above a critical value $\Delta\mu_c$ for oscillations to occur, which is also the case for the standard Brusselator. In our modified model, the threshold $\Delta\mu_c$ depends on the parameters Λ and γ . Moreover, γ and Λ must be above certain thresholds for oscillations to set in; their specific critical values depend on the system parameters. In Fig. 4(a) and (b), we observe a decrease in the precision of oscillations for increasing Λ . As Λ increases, so does $\Delta\mu_c$, which causes \mathcal{N} to decrease and, in Fig. 4(b), even to vanish. Most remarkably, we find that $\mathcal{N}(\Lambda)$ approaches $\mathcal{N}(\Lambda \rightarrow \infty)$, which corresponds to the infinite reservoir from above. This result implies that for values of $\Delta\mu$ for which both models show oscillations, the oscillations driven by finite reservoirs can show higher precision than the ones with ideal reservoirs despite having larger fluc-

tuations. In addition, the model with finite reservoirs can show oscillations when the one with ideal reservoirs does not. In this sense, the finite reservoirs outperform the infinite ones.

Second, for finite reservoirs, oscillations can vanish when $\Delta\mu$ and γ are too large, see Fig. 3(c). As shown in Fig. 4(c) and (d), \mathcal{N} reaches a maximum and vanishes for large $\Delta\mu$ and γ . For an explanation of this surprising effect, we plot the phase portrait of the deterministic system in Fig. 5. In the steady-state, the deterministic system will remain on a limit cycle as shown in Fig. 5(a). This is no longer the case for the stochastic system which can explore larger cycles due to fluctuations. We illustrate this by perturbing a deterministic trajectory located on the limit cycle as indicated by the red arrow. Where streamlines are dense, such a pertur-

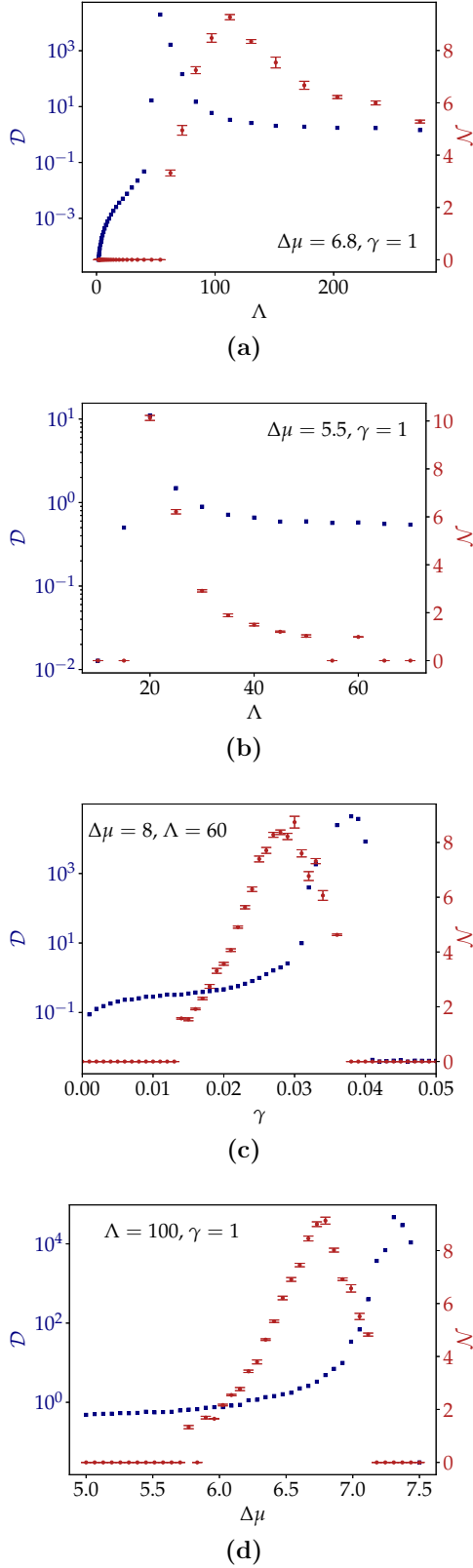


FIG. 4. Comparison between the diffusion coefficient (blue squares) the number of coherent oscillations (red circles) as a function of the reservoir size Λ for (a) and (b), pumping timescale γ for (c) and thermodynamic force $\Delta\mu$ for (d). The error bars result from fitting Eq. (10).

bation can lead to a large change in the trajectory. The system goes through a large cycle before converging back to the limit cycle.

For the stochastic system, fluctuations are constantly perturbing the trajectory, which stochastically leads to large cycles. Their appearance results in a decrease in the number of coherent oscillations as these large cycles are no longer coherent with the oscillations in the limit cycle. As $\Delta\mu$ and γ are increased, transitions from the inner limit cycle onto a larger cycle are more likely to happen. The effect of varying Λ is shown in Fig. 5 (b)-(d). The bifurcation diagram Fig. 5 (d) shows the X -value of fixed-point solutions of the deterministic system. In the green region for $\Lambda \gtrsim 67$, oscillations occur around the unstable fixed-point. As Λ decreases below $\Lambda \simeq 67$, the system undergoes a homoclinic bifurcation⁵¹ through which the stable limit cycle disappears and trajectories end at a stable fixed-point as shown in Fig. 5 (b) and (c). It is interesting to note that in Fig. 4 the largest coherence occurs closer to the homoclinic bifurcation than to the Hopf bifurcation. This is due to the fact that at the homoclinic bifurcation the oscillation amplitude is larger, making fluctuations less noticeable.

For the parameter range plotted in Fig. 4 as indicated in Fig. 3, the oscillations of $n_X(t)$ and $n_Y(t)$ are stabilized by oscillations in the number of A and B molecules in the reservoirs as shown in Fig. 2 (a). Oscillations can occur because the pumping mechanism Eq. (4) does not attempt to keep the reservoir concentrations fixed. Rather, it restores the ratio of the bath concentrations to a fixed value given by $\Delta\mu$, since $[A]/[B]$ is proportional to $e^{-\Delta\mu}$ according to the local detailed balance condition Eq. (5). At small bath scales Λ , from the systems perspective bath oscillations become noticeable and could qualitatively explain the improved precision of finite reservoirs in Fig. 4 (a).

IV. CONCLUSION

We have introduced a simple model for the role of finite reservoirs in chemical reaction networks. To uphold a NESS, we have introduced a pumping mechanism, which implicitly still assumes an ideal reservoir as a source of constant $\Delta\mu$. The crucial point of our model, however, is that the number of A and B molecules required as a source for generating oscillations in X and Y are finite and fluctuating. This model thus better reflects the real conditions in biological systems than the usual assumption of infinite reservoirs. We have considered the simplest possible mechanism, a first-order chemical reaction converting species between reservoirs. This class of reservoirs is characterized by three parameters: the thermodynamic force $\Delta\mu$, the bath scale Λ , which relates the reservoir size to the rest of the system and the timescale of the pumping mechanism γ . The ideal reservoirs are recovered in the limit $\Lambda \rightarrow \infty$ (independently of γ).

As a case study, we have investigated a biochemical os-

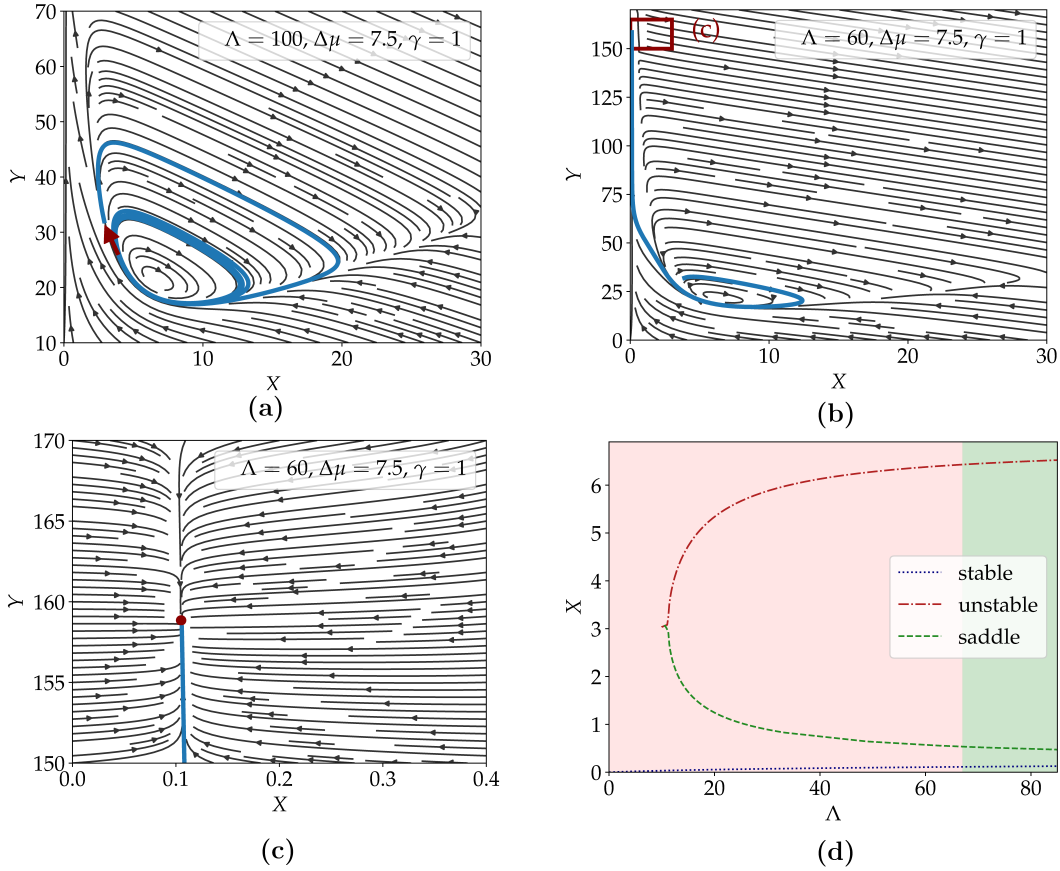


FIG. 5. Phase portrait in the X-Y plane. (a) Emergence of additional larger cycles. We perturb the deterministic system along the red arrow. The system then goes through a larger cycle and converges back to the limit cycle (exemplary trajectory in blue). (b) Trajectory reaches a stable fixed-point located in the red square as Λ decreases. (c) Enlargement of the red square from (b). It shows the locally stable fixed-point in red. (d) Bifurcation diagram. The fixed-points can be either stable (dotted blue), unstable (dashdotted red) or saddle points (dashed green). In the green region oscillations occur around the unstable point. At the red-green boundary a homoclinic bifurcation takes place.

cillator, the Brusselator, with this simple pumping mechanism. We quantify the precision of oscillations by measuring the number of coherent oscillations and the diffusion coefficient associated with the pump. We find that the occurrence of oscillations critically depends on all of the parameters $\Delta\mu$, γ and Λ , in other words, oscillations can only occur if the thermodynamic force, the size of the chemostats and the pumping speed are within a certain range. Most surprisingly, the highest precision of oscillations occurs at finite parameters $\Delta\mu$, γ and Λ . This is in contrast to the Brusselator model³³ and other unicyclic models^{49,50} considered in the previous literature, where the precision of oscillations monotonically increases with the control parameter $\Delta\mu$. As a main result, we find that a system with finite reservoirs can outperform one with ideal reservoirs despite having larger fluctuations.

Our framework could be extended by considering more sophisticated pumping mechanisms. It would be interesting to consider the ATP synthase, for which thermodynamically consistent models exist²⁷. Specifically, it would be interesting to study the relation between the

efficiency of the motor and the precision of oscillations. Another interesting case is the coupling of biochemical clocks which can be optimized to maximize the precision of oscillations³⁷. Moreover, it has been shown recently that periodically driven oscillator can achieve better coherence than under NESS conditions⁵². It would be interesting to investigate how fluctuations in the periodic protocol affect the precision of oscillations. Finally, we expect that considering finite reservoirs may show further surprises for biochemical systems beyond the enhanced precision of oscillations discovered here.

DATA AVAILABILITY STATEMENT

The data that support the findings of this study are available from the corresponding author upon reasonable request.

¹J. Howard, *Mechanics of Motor Proteins and the Cytoskeleton*, 1st ed. (Sinauer, New York, 2001).

²M. Schliwa, *Molecular Motors* (Wiley-VCH, Weinheim, 2003).

- ³R. Philips, J. Kondev, and J. Theriot, *Physical Biology of the Cell*, 1st ed. (Garland Science, Taylor & Francis Group, LLC, New York, 2009).
- ⁴B. Alberts, A. Johnson, J. Lewis, M. Raff, K. Roberts, and P. Walter, *Molecular Biology of the Cell*, 6th ed. (Garland Science, Taylor & Francis Group, LLC, New York, 2015).
- ⁵A. Goldbeter and M. J. Berridge, *Biochemical Oscillations and Cellular Rhythms: The Molecular Bases of Periodic and Chaotic Behaviour* (Cambridge University Press, 1996).
- ⁶M. Nakajima, K. Imai, H. Ito, T. Nishiwaki, Y. Murayama, H. Iwasaki, T. Oyama, and T. Kondo, *Science* **308**, 414 (2005).
- ⁷E. Fischer-Friedrich, G. Meacci, J. Lutkenhaus, H. Chaté, and K. Kruse, *Proc. Natl. Acad. Sci. USA* **107**, 6134 (2010).
- ⁸J. Halatek and E. Frey, *Cell. Rep.* **1**, 741 (2012).
- ⁹L. Xiong and G. Lan, *PLoS Comput. Biol.* **11**, 1 (2015).
- ¹⁰F. Wu, J. Halatek, M. Reiter, E. Kingma, E. Frey, and C. Dekker, *Mol. Syst. Biol.* **12**, 873 (2016).
- ¹¹J. Denk, S. Kretschmer, J. Halatek, C. Hartl, P. Schwill, and E. Frey, *Proc. Natl. Acad. Sci. USA* **115**, 4553 (2018).
- ¹²E. Mizuno-Yamasaki, F. Rivera-Molina, and P. J. Novick, *Annu. Rev. Biochem.* **81**, 637 (2012).
- ¹³Y. Suda, K. Kurokawa, R. Hirata, and A. Nakano, *Proc. Natl. Acad. Sci. USA* **110**, 18976 (2013).
- ¹⁴W. M. Bement, M. Leda, A. M. Moe, A. M. Kita, M. E. Larson, A. E. Golding, C. Pfeuti, K.-C. Su, A. L. Miller, A. B. Goryachev, and G. von Dassow, *Nat. Cell Biol.* **17**, 14711483 (2015).
- ¹⁵A. Ehrmann, B. Nguyen, and U. Seifert, *J. R. Soc. Interface* **16**, 20190198 (2019).
- ¹⁶F. Westheimer, *Science* **235**, 1173 (1987).
- ¹⁷S. C. L. Kamerlin, P. K. Sharma, R. B. Prasad, and A. Warshel, *Q. Rev. Biophys.* **46**, 1132 (2013).
- ¹⁸P. Rich, *Biochem. Soc. Trans.* **31**, 1095 (2003).
- ¹⁹L. Stryer, J. Berg, J. Tymoczko, and G. Gatto, *Biochemistry*, 7th ed. (W. H. Freeman and Company, New York, 2012).
- ²⁰P. D. Boyer, *Annu. Rev. Biochem.* **66**, 717 (1997).
- ²¹W. Junge and N. Nelson, *Annu. Rev. Biochem.* **84**, 631 (2015).
- ²²S. Toyabe, T. Okamoto, T. Watanabe-Nakayama, H. Taketani, S. Kudo, and E. Muneyuki, *Phys. Rev. Lett.* **104**, 198103 (2010).
- ²³S. Toyabe, T. Watanabe-Nakayama, T. Okamoto, S. Kudo, and E. Muneyuki, *Proc. Natl. Acad. Sci. U. S. A.* **108**, 17951 (2011).
- ²⁴S. Toyabe and E. Muneyuki, *New J. Phys.* **17**, 015008 (2015).
- ²⁵P. Gaspard and E. Gerritsma, *J. Theor. Biol.* **247**, 672 (2007).
- ²⁶E. Gerritsma and P. Gaspard, *Biophys. Rev. Lett.* **05**, 163 (2010).
- ²⁷E. Zimmermann and U. Seifert, *New J. Phys.* **14**, 103023 (2012).
- ²⁸A. Carcaterra and A. Akay, *Phys. Rev. E* **84**, 011121 (2011).
- ²⁹A. Carcaterra and A. Akay, *Phys. Rev. E* **93**, 032142 (2016).
- ³⁰H. Qian and M. Qian, *Phys. Rev. Lett.* **84**, 2271 (2000).
- ³¹Y. Cao, H. Wang, Q. Ouyang, and Y. Tu, *Nat. Phys.* **11**, 772 (2015).
- ³²A. C. Barato and U. Seifert, *Phys. Rev. E* **95**, 062409 (2017).
- ³³B. Nguyen, U. Seifert, and A. C. Barato, *J. Chem. Phys.* **149**, 045101 (2018).
- ³⁴C. Fei, Y. Cao, Q. Ouyang, and Y. Tu, *Nat. Commun.* **9**, 1434 (2018).
- ³⁵T. Herpich, J. Thingna, and M. Esposito, *Phys. Rev. X* **8**, 031056 (2018).
- ³⁶R. Marsland, W. Cui, and J. M. Horowitz, *J. R. Soc. Interface* **16**, 20190098 (2019).
- ³⁷D. Zhang, Y. Cao, Q. Ouyang, and Y. Tu, *Nat. Phys.* **16**, 95 (2020).
- ³⁸C. del Junco and S. Vaikuntanathan, *Phys. Rev. E* **101**, 012410 (2020).
- ³⁹C. del Junco and S. Vaikuntanathan, *J. Chem. Phys.* **152**, 055101 (2020).
- ⁴⁰H. Qian, S. Saffarian, and E. L. Elson, *Proc. Natl. Acad. Sci. USA* **99**, 10376 (2002).
- ⁴¹G. Nicolis and J. Turner, *Physica A* **89**, 326 (1977).
- ⁴²R. Lefever, G. Nicolis, and P. Borckmans, *J. Chem. Soc., Faraday Trans. 1* **84**, 1013 (1988).
- ⁴³U. Seifert, *Rep. Prog. Phys.* **75**, 126001 (2012).
- ⁴⁴N. G. van Kampen, *Stochastic Processes in Physics and Chemistry*, 3rd ed., North-Holland Personal Library (Elsevier, Amsterdam, 2007).
- ⁴⁵D. T. Gillespie, *J. Phys. Chem.* **81**, 2340 (1977).
- ⁴⁶A. C. Barato and U. Seifert, *J. Phys. Chem. B* **119**, 6555 (2015).
- ⁴⁷T. R. Gingrich, J. M. Horowitz, N. Perunov, and J. L. England, *Phys. Rev. Lett.* **116**, 120601 (2016).
- ⁴⁸U. Seifert, *Annu. Rev. Condens. Matter Phys.* **10**, 171 (2019).
- ⁴⁹A. C. Barato and U. Seifert, *Phys. Rev. X* **6**, 041053 (2016).
- ⁵⁰H. Wierenga, P. R. ten Wolde, and N. B. Becker, *Phys. Rev. E* **97**, 042404 (2018).
- ⁵¹S. Strogatz, *Nonlinear Dynamics and Chaos: With Applications to Physics, Biology, Chemistry, and Engineering*, 2nd ed. (Westview Press, 2015).
- ⁵²L. Oberreiter, U. Seifert, and A. C. Barato, *Phys. Rev. E* **100**, 012135 (2019).